JOURNAL OF MATERIALS SCIENCE 28 (1993) 6233–6245

Stress transfer in the fibre fragmentation test

Part I *An improved analysis based on a shear strength criterion*

JANG-KYO KIM*, LIMIN ZHOU, YIU-WING MAI
Centre for Advanced Materials Technology, Department of Mechanical and Mechatronic Engineering, University of Sydney, Sydney, NSW 2006, Australia

An improved micromechanics model has been developed of the stress transfer for a single fibre embedded in a matrix subjected to uniaxial loading. Debond crack growth is analysed based on the shear strength criterion such that when the interfacial shear stress reaches the shear bond strength, debonding occurs; and the average strength concept based on Weibull statistics is considered for fibre fragmentation. The influences of the interfacial shear bond strength and the fibre strength on the stress distributions in the composite constituents are evaluated. Depending on the relative magnitudes of these two strength parameters and given the elastic constants and geometric factors, three distinct conditions of the fibre–matrix interface are properly identified which include full bonding, partial debonding and full frictional bonding. Also quantified are the necessary criteria which must be satisfied in order for each interface condition to be valid. Finally, the mean fibre fragment length is predicted as a function of applied strain using a model composite of carbon fibre–epoxy matrix. The parametric study suggests that the critical transfer length predicted when the applied strain (or stress) required for further fibre fragmentation approaches infinity, can be regarded as a material constant, which is the sum of the bonded and the debonded lengths for the model composite.

1. Introduction

Over the past decades a significant effort has been put into understanding the stress transfer in the fibre fragmentation test as a means of evaluating the bond quality at the fibre–matrix interface [1]. This endeavour has been prompted by the rapid development of technologically important fibres and matrix materials and the corresponding new surface treatment techniques of various nature which have to be compatible with the composite fabrication processes and actual service environments.

Since the early work of Cox [2] there have been a number of micromechanics models developed to predict the stress state, particularly near the broken fibre ends, and ultimately to measure the interface bond strength. Although some recent works have been directed towards the establishment of more reliable models by incorporating statistic aspects of fibre fragment length [3, 4] and fibre strength [5–9], as well as plastic deformation of matrix material [10–12] occurring during the fibre fragmentation test, the basic form of relationship between the critical transfer length and the shear strength at the interface, whether bonded or debonded, remain virtually unchanged from the solution originally proposed by Kelly and Tyson [13]. Further, in contrast to the conventional opinion of either complete bonding or complete debonding (or complete matrix yielding whichever occurs first), a clearly emerging view in recent years is that there are both bonded and debonded interfaces present simultaneously during the fibre fragmentation process [14–18].

In this context, a comprehensive treatment is given [19] in a micromechanics analysis of the fibre fragmentation test on the basis of the concept of fracture mechanics. It is assumed there that the debond crack propagates along the interface when the differential potential energy stored in the constituents of the composites is satisfied with respect to the interfacial fracture toughness, and the fibre breaks when the maximum fibre axial stress occurring at the fibre centre exceeds the average tensile strength. Considering the partially debonded interface as the most general case, a parametric study has been performed for a model composite of carbon fibre–epoxy matrix. It is noted that there is a characteristic applied stress (or strain) below which no debonding takes place. With increasing applied stress from this value the debond length increases towards an asymptotic value while the bond length decreases relatively slowly. The sum of the asymptotic debond and bond lengths can be regarded as the shortest mean fibre fragmentation length, so-called critical transfer length, which can be obtained theoretically for given properties of the composite constituents and the interface. In practice, however, a significantly higher value is expected for the

Present address: Engineering Program, The Faculties, Australian National University, Canberra, ACT 0200 Australia.

0022–2461

critical transfer length due to the experimental difficulties associated with the limited ductility of the matrix material.

Although a fracture mechanics approach in general deals with a more fundamental aspect of the interface debond problem for a given loading configuration [20, 21], a shear strength criterion has an important advantage in that the interfacial shear strength, whether for the bonded or debonded regions, can be directly determined from the experimental results of the fibre fragmentation test. (This will be discussed in full details in Part II of this paper [22].) Therefore, in the present paper, an improved micromechanics analysis is developed of the fibre fragmentation test based on the shear strength criterion for the interfacial debonding. Depending on the interface properties and the fibre tensile strength for given elastic constants of the composite constituents, three distinct conditions for the fibre–matrix interface are identified, i.e. full bonding, partial debonding and full frictional bonding. A particular emphasis is placed on the identification of the specific criteria required to satisfy each interface condition. The approximate analysis given in the present model leads to relatively simple closed-form equations for all basic solutions for the stress distributions in the constituents, the external stress required for debonding or fibre fragmentation, and the mean fibre fragmentation length for the three different interface conditions.

2. Theoretical analysis

2.1. Basic governing conditions

The geometry of the model and the governing conditions adopted in the present analysis are essentially the same as those employed in a previous work [19]. The shear-lag model shown in Fig. 1 contains a single fibre (of radius a) which is embedded at the centre of a coaxial cylindrical shell of matrix (of an outer radius b). L is half fibre length with partial debonded regions each of length, l, from both fibre ends. A set of cylindrical coordinates (r, θ, z) is selected so that the z-axis corresponds to the axis of the fibre and r is the distance from the fibre axis. In the fibre fragmentation test, a tensile stress, σ, is applied to the matrix at the remote ends, and the stress is transferred to the fibre across the fibre–matrix interface. If we assume that the fibre ends are bonded to the matrix at $z = \pm L$, stresses can be transferred from the matrix to the fibre through continuity at the fibre ends. However, this condition is only valid until the maximum fibre axial stress reaches the fibre tensile strength (corresponding to the initial fibre length $2L$) after which the fibre for the first time breaks into two pieces. As the applied stress is further increased the fibre breaks into gradually smaller segments until no more breaks occur. The mean value of the fibre fragment lengths at this point is called the critical transfer length. Because of the random nature of the flaw size and spatial distribution along the fibre length which causes the fibre segment lengths to be non-uniform, there may exist asymmetric distributions of stresses. For simplicity, it is assumed here that the fibre ends are debonded from the matrix so that there is no stress transfer through the ends (i.e. $\sigma_f^z = 0$ at $z = \pm L$). The mode of deformation is assumed symmetric about the fibre axis (i.e. axisymmetric) as well as about the plane perpendicular to the centre of the fibre at $z = 0$. Hence the stress components $(\sigma^r, \sigma^\theta, \sigma^z, \tau^{rz})$ and the displacement components (u^r, u^z) are all independent of the tangential coordinate, θ. The remaining stress and displacement components are all zero.

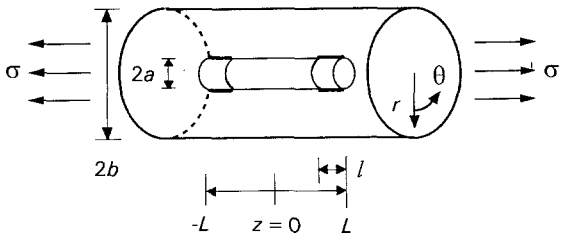

Figure 1 A schematic drawing of the partially debonded fibre in the fibre fragmentation model.

2.2. Solutions for the stress components in the bonded region: $-(L-l) \leqslant z \leqslant (L-l)$

The solutions for the fibre axial stress, $\sigma_f^z(z)$, and the interfacial shear stress, $\tau_i^{rz}(z)$, are obtained with given boundary conditions in Appendix 1

$$\sigma_f^z(z) = \left(\frac{1+\gamma}{\alpha+\gamma}\right)\left\{1 - \frac{\cosh(\beta_2 z)}{\cosh[\beta_2(L-l)]}\right\}\sigma + \left\{\frac{\cosh(\beta_2 z)}{\cosh[\beta_2(L-l)]}\right\}\sigma_l \quad (1)$$

$$\tau_i^{rz}(z) = \left(\frac{a\beta_2}{2}\right)\left[\left(\frac{1+\gamma}{\alpha+\gamma}\right)\sigma - \sigma_l\right]\frac{\sinh(\beta_2 z)}{\cosh[\beta_2(L-l)]} \quad (2)$$

where

$$\beta_2^2 = \frac{(b^2-a^2)(1+\alpha/\gamma)}{(1+\gamma)[b^4\ln(b/a) - (b^2-a^2)^2/2 - (b^4-a^4)/4]}. \quad (3)$$

$\gamma = a^2/(b^2-a^2)$ and $\alpha = E_m/E_f$, which are the volume ratio of the fibre to the matrix and the Young's modulus ratio of the matrix to the fibre, respectively. σ_l is the crack tip debond stress at the boundary between the bonded and debonded regions (Fig. 1). If it is assumed for a special case that the fibre–matrix interface is completely bonded (i.e. the debond crack tip stress $\sigma_l = 0$ when $l = 0$), the above equations become

$$\sigma_f^z(z) = \left(\frac{1+\gamma}{\alpha+\gamma}\right)\left[1 - \frac{\cosh(\beta_2 z)}{\cosh(\beta_2 L)}\right]\sigma \quad (4)$$

$$\tau_i^{rz}(z) = \left(\frac{a\beta_2}{2}\right)\left(\frac{1+\gamma}{\alpha+\gamma}\right)\left[\frac{\sinh(\beta_2 z)}{\cosh(\beta_2 L)}\right]\sigma \quad (5)$$

2.3. Solutions for the stress components in the debonded region: $-L \leqslant z \leqslant -(L-l)$ and $(L-l) \leqslant z \leqslant L$

The solutions for the fibre axial stress, $\sigma_f^z(z)$, and the interfacial shear stress, $\tau_i^{rz}(z)$, are obtained with appro-

priate boundary conditions in Appendix 2

$$\sigma_f^z(z) = \frac{B_3}{B_2}[D_1 \exp(m_2 z) + D_2 \exp(m_1 z)] + \sigma_l[D_3 \exp(m_2 z) + D_4 \exp(m_1 z)] \quad (6)$$

$$\tau_i^{rz}(z) = -\frac{a}{2}\left\{\frac{B_3}{B_2}[m_2 D_1 \exp(m_2 z) + m_1 D_2 \exp(m_1 z)] + \sigma_l[m_2 D_3 \exp(m_2 z) + m_1 D_4 \exp(m_1 z)]\right\} \quad (7)$$

where the non-dimensional coefficients D_1, D_2, D_3 and D_4 are given by

$$D_1 = \frac{1 - \exp(-m_1 l)}{\exp(m_2 L)[\exp(-m_1 l) - \exp(-m_2 l)]} \quad (8)$$

$$D_2 = -\frac{1 - \exp(-m_2 l)}{\exp(m_1 L)[\exp(-m_1 l) - \exp(-m_2 l)]} \quad (9)$$

$$D_3 = -\frac{1}{\exp(m_2 L)[\exp(-m_1 l) - \exp(-m_2 l)]} \quad (10)$$

$$D_4 = \frac{1}{\exp(m_1 L)[\exp(-m_1 l) - \exp(-m_2 l)]} \quad (11)$$

Also

$$m_1 = -\frac{B_1 + (B_1 + 4\lambda B_1)^{1/2}}{2} \quad (12)$$

$$m_2 = \frac{-B_1 + (B_1 + 4\lambda B_1)^{1/2}}{2} \quad (13)$$

where

$$B_1 = \frac{\alpha \nu_f + \gamma \nu_m}{\nu_m(\alpha + \gamma)} \frac{\beta_2}{\lambda} \quad (14)$$

$$B_2 = -\lambda B_1 \quad (15)$$

$$B_3/B_2 = \frac{(1 + \gamma)\nu_m}{\alpha \nu_f + \gamma \nu_m} \sigma + \omega \bar{\sigma} \quad (16)$$

λ is the reciprocal length giving the effective frictional shear stress transfer and $\bar{\sigma}$ is the asymptotic debond stress for long fibre length. These parameters are related to the coefficient of friction, μ, and the residual clamping stress, q_0, as for the fibre pull-out model [23]

$$\lambda = 2\mu k/a \quad (17)$$

$$\bar{\sigma} = -q_0/\omega k \quad (18)$$

where $\omega = \alpha \nu_f/(\alpha \nu_f + \gamma \nu_m)$ and $k = (\alpha \nu_f + \gamma \nu_m)/[\alpha(1 - \nu_f) + 1 + \nu_m + 2\gamma]$.

For a given debond length, l, relative to L, determination of the crack tip debond stress, σ_l, is subject to the condition that the fibre axial strain is equivalent to the matrix axial strain at the boundary between the bonded and debonded regions (i.e. $\partial u_f^z(z)/\partial z = \partial u_m^z(a, z)/\partial z$ at $z = \pm(L - l)$). Within the debonded region the matrix axial strain at the interface is greater than the fibre axial strain due to the relative slip between fibre and matrix. Therefore, combining Equations A1, A2 and A15 at the boundary, σ_l is obtained from

$$\sigma_l = -\frac{\sigma(1 + \gamma)\nu_m n_1 + \bar{\sigma}\alpha\nu_f(n_1 + \lambda)}{\alpha\lambda(\nu_m - \nu_f) + (\alpha\nu_f + \gamma\nu_m)n_2} \quad (19)$$

where

$$n_1 = \frac{-m_1 \exp(-m_1 l) + m_2 \exp(-m_2 l) + (m_1 - m_2)\exp[-(m_1 + m_2)l]}{\exp(-m_1 l) - \exp(-m_2 l)} \quad (20)$$

$$n_2 = \frac{m_1 \exp(-m_1 l) - m_2 \exp(-m_2 l)}{\exp(-m_1 l) - \exp(-m_2 l)} \quad (21)$$

2.4. Fibre–matrix interface debond criterion

In the shear strength criterion, the debond crack propagates when the maximum interfacial shear stress at the debond crack tip $z = \pm(L - l)$ reaches the shear bond strength, τ_b (which is assumed constant), i.e.

$$\tau_i^{rz}(L - l) = \tau_b \text{ (or, } \tau_i^{rz}(-L + l) = -\tau_b) \quad (22)$$

By substituting Equation 22 into Equation 2, the debond crack tip stress, σ_l, is expressed as a function of the material properties and the external applied stress, σ. Thus

$$\sigma_l = \left(\frac{1 + \gamma}{\alpha + \gamma}\right)\sigma - \left(\frac{2\tau_b}{a\beta_2}\right)\coth[\beta_2(L - l)] \quad (23)$$

Therefore, by combining Equations 19 and 23, one can derive the stress applied to the matrix at the remote ends, $\sigma = \sigma_{od}$, for debond crack propagation

$$\sigma_{od} = \frac{(2n_3/a\beta_2)\tau_b \coth[\beta_2(L - l)] - \alpha\nu_f(n_1 + \lambda)\bar{\sigma}}{(1 + \gamma)[n_3/(\alpha + \gamma) + \nu_m n_1]} \quad (24)$$

where

$$n_3 = \alpha\lambda(\nu_m - \nu_f) + n_2(\alpha\nu_f + \gamma\nu_m) \quad (25)$$

2.5. Fibre fragmentation criterion

When the applied stress is sufficient to cause the maximum fibre axial stress to exceed the local fibre tensile strength, the fibre fractures. In the present study, a fibre tensile strength model analogous to that employed in the previous study [19] is used to predict the average strength of the fibre, $\sigma_{TS}(2L_g)$, corresponding to a given gauge length, $2L_g$, based on the Weibull probability of failure [24]

$$\sigma_{TS}(2L_g) = \sigma_u(2L_g)^{-1/m}\Gamma(1 + 1/m) \quad (26)$$

where m and σ_u are the Weibull modulus and the scale factor, and Γ is the gamma function. Therefore, the average tensile strength of a fibre segment of length, $2L$, is given by

$$\sigma_{TS}(2L) = \sigma_{TS}(2L_g)[L_g/L]^{1/m} \quad (27)$$

Because the fibre axial stress, $\sigma_f^z(z)$, is maximum at the centre of the embedded fibre

$$\sigma_f^z(0) = \sigma_{TS}(2L) \tag{28}$$

Therefore, by substituting Equation 28 into Equation 1, the fibre fragmentation criterion is derived in terms of the external stress, $\sigma = \sigma_{of}$, i.e.

$$\sigma_{of} = \left(\frac{\alpha+\gamma}{1+\gamma}\right)\frac{\sigma_{TS}(2L)\cosh[\beta_2(L-l)] - \sigma_l}{\cosh[\beta_2(L-l)] - 1} = \left(\frac{\alpha+\gamma}{1+\gamma}\right)\{\sigma_{TS}(2L) + (2\tau_b/a\beta_2)\operatorname{cosech}[\beta_2(L-l)]\} \tag{29}$$

3. Three cases of interfacial bonding

Depending on the applied stress relative to the fibre tensile strength and the interfacial properties (which include the interfacial shear bond strength, τ_b, in the bonded region, and the coefficient of friction, μ, and the residual clamping stress, q_0, in the bonded region) for given elastic properties of the constituents and the geometric factors of the fibre fragmentation model, three distinct cases are possible with regard to the fibre–matrix interface condition: (i) full bonding; (ii) partial debonding; and (iii) complete debonding or full frictional bonding [18]. In this section, the conditions required to satisfy each interface state are systematically identified in terms of the relationship between the applied stress and the properties of the constituents and the interface. The stress distributions in the constituents are characterized for each interface state, and the important factors governing the stress fields are identified. Therefore, the fibre fragmentation criterion is applied to derive the mean fibre fragment length, $2L$, as a function of the applied stress. Specific results are calculated based on the solutions derived in the previous sections for the model composite of a carbon fibre in an epoxy matrix [19], and whose mechanical properties are given in Table I. Also included in the table are the Weibull statistics of the fibre tensile strength. Unless otherwise specified, the interfacial properties used for the numerical calculations are $\tau_b = 72.7$ MPa, $\mu = 1.5$ and $q_0 = -10$ MPa which are determined from the single-fibre pull-out test [20, 21].

3.1. Full bonding

We first consider the case when the interface is perfectly bonded over the full fibre length where elastic stress is transferred across the interface. The fibre axial stress, $\sigma_f^z(z)$, and the interfacial shear stress, $\tau_i^{rz}(z)$, normalized with the applied stress, σ, are plotted along the normalised axial direction, z/a, as shown in Fig. 2. Because varying the fibre length only changes the effective length of the central part of the curve whose stress values are almost constant, those for only one fibre length, $2L = 2$ mm, are plotted. Corresponding plots for the negative axial direction can also be shown by symmetry of the axial stress and anti-symmetry of the interface shear stress with respect to the fibre centre, $z = 0$. The effect of modulus ratio, E_m/E_f, is clearly visualized on the stress distribution. Both the maximum values of the fibre axial stress and the interfacial shear stress, which are obtained in the centre and at the ends of the fibre, respectively, increase with decreasing modulus ratio, E_m/E_f, at a given applied stress. This means that the efficiency of stress transfer across the fibre–matrix interface increases with decreasing E_m/E_f. That is, a lower external stress is required for fibre fragmentation or debond initiation for a composite with a smaller value of E_m/E_f if other parameters remain the same.

The fibre–matrix interface is fully bonded so long as the maximum interfacial shear stresses obtained at the fibre ends ($z = \pm L$) are smaller than the interface shear bond strength, τ_b, which is assumed to be a material constant. Hence

$$\tau_i^{rz}(L) < \tau_b \quad (\text{or, } \tau_i^{rz}(-L) > -\tau_b) \tag{30}$$

Combination of Equations 5 and 30 gives

$$\sigma < \left(\frac{\alpha+\gamma}{1+\gamma}\right)\left(\frac{2}{a\beta_2}\right)\tau_b\coth(\beta_2 L) \tag{31}$$

Under this circumstance, the external stress corresponding to the fibre fragmentation, σ_{of}, is obtained from Equation 4

$$\sigma_{of} = \left(\frac{\alpha+\gamma}{1+\gamma}\right)\sigma_{TS}(2L)\frac{\cosh(\beta_2 L)}{\cosh(\beta_2 L) - 1} \tag{32}$$

Because Equation 32 also has to satisfy the condition for full bonding at the interface governed by Equation 31, fibre fragmentation takes place when

$$\tau_b > \left(\frac{a\beta_2}{2}\right)\frac{\sinh(\beta_2 L)}{\cosh(\beta_2 L) - 1}\sigma_{TS}(2L) \tag{33}$$

The curve in Fig. 3a shows the critical combination of the interfacial bond strength, τ_b, and the fibre length, $2L$, which allows the initial debonding at the interface. Therefore, the areas above and below the curve represent, respectively, full bonding and partial debonding at the interface. The average fibre tensile strength was estimated based on Equation 27 with the Weibull parameters given in Table I. Therefore, for a composite with a given value for τ_b, it is possible to evaluate the minimum fibre length, $(2L)_d$, until which fibre fragmentation takes place whilst the interface is

TABLE I Mechanical/interface properties of carbon fibre–epoxy matrix composites and the Weibull parameters of fibre tensile strength

Mechanical/interface properties	Weibull parameters
$E_f = 230$ GPa, $E_m = 3.0$ GPa, $\nu_f = 0.2$, $\nu_m = 0.4$ $\tau_b = 72.7$ MPa, $\mu = 1.5$, $q_0 = -10$ MPa	$2L_g = 12$ mm, $\sigma_{TS}(2L_g) = 2.35$ GPa, $m = 3.8$, $\sigma_u = 5.0$

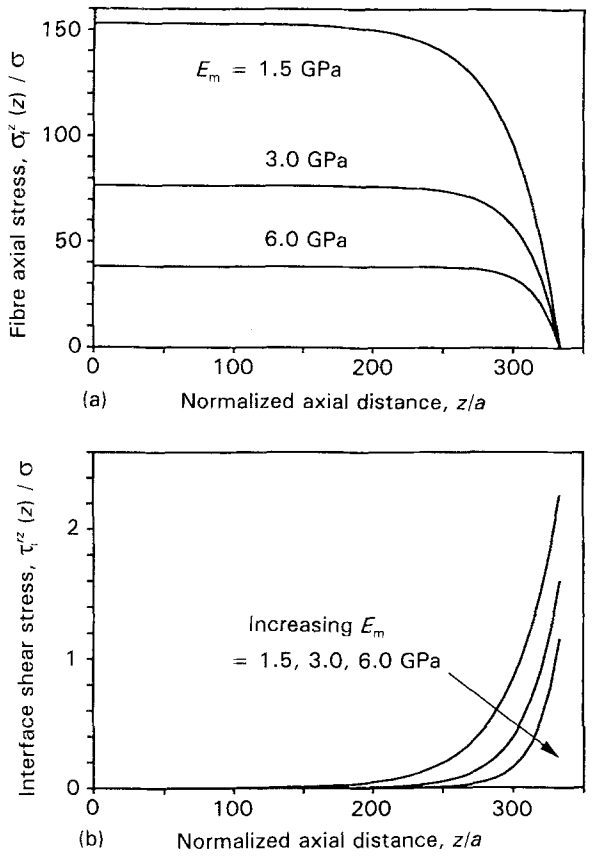

Figure 2 Distribution of (a) normalized fibre axial stress, σ_f^z/σ, and (b) normalized interface shear stress, τ_i^{rz}/σ, along the fibre axis, z/a, for elastic moduli $E_m = 1.5$, 3.0 and 6.0 GPa with a constant $E_f = 230$ GPa and $2L = 2$ mm.

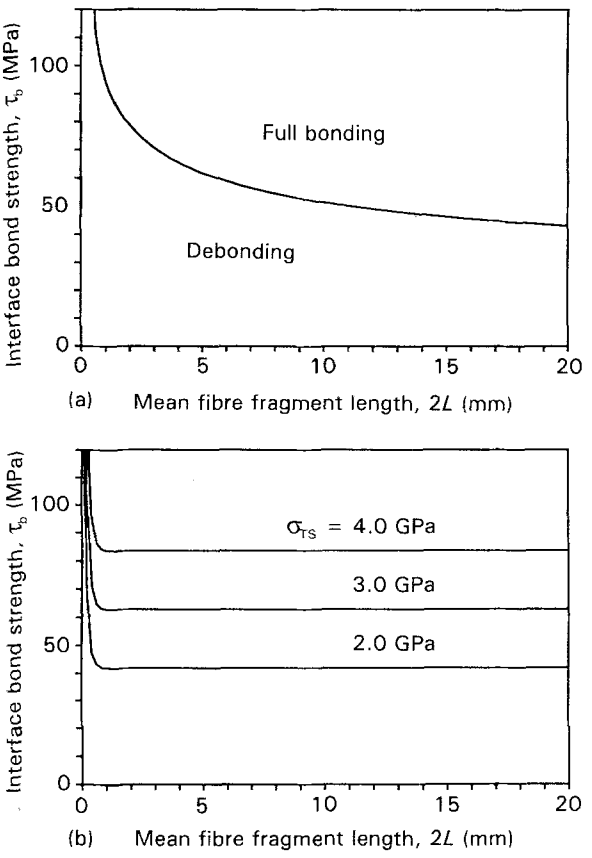

Figure 3 Plot of interface shear bond strength, τ_b, as a function of fibre length, $2L$, calculated based on Equation 33: (a) for variable average tensile strength, $\sigma_{TS}(2L)$, according to the Weibull parameters in Table I; and (b) for constant fibre tensile strengths $\sigma_{TS} = 2.0$, 3.0 and 4.0 GPa.

fully bonded. For example, $(2L)_d \approx 2.71$ mm for $\tau_b = 72.7$ MPa. If τ_b is raised to 100 MPa, or reduced to 50 MPa, the corresponding values for $(2L)_d$ vary inversely, giving $(2L)_d \approx 0.83$ and 11.25 mm, respectively.

Further, if the fibre tensile strength is assumed constant independent of fibre length, τ_b is almost invariant with $2L$ over the whole range of fibre lengths, except for very short fibre lengths where τ_b decreases dramatically with $2L$ (Fig. 3b). Increasing the fibre tensile strength also increases the corresponding constant τ_b values. This implies that for a given τ_b whether fibre fragmentation can occur or not, depends predominantly on the constant fibre tensile strength, and once the fibre initially fractures it continues until the fibre length becomes very short. For example, the characteristic fibre lengths for initial debonding $2L)_d \approx 0.19$ and 0.39 mm are obtained for $\sigma_{TS} = 2.0$ and 3.0 GPa, respectively, if $\tau_b = 72.7$ MPa. For the same interfacial bond strength, fibre fragmentation is not possible if σ_{TS} is greater than approximately 3.5 GPa in this full bond model (see Fig. 3b).

Once the requirements for full bonding are satisfied, the mean fibre fragmentation length, $2L$, can be determined as a function of the external stress, σ_{of}, and the fibre tensile strength, $\sigma_{TS}(2L)$, by rearranging Equation 32

$$2L = \left(\frac{2}{\beta_2}\right)\cosh^{-1}\left\{\frac{\sigma_{of}}{\sigma_{of} - [(\alpha+\gamma)/(1+\gamma)]\sigma_{TS}(2L)}\right\} \quad (34)$$

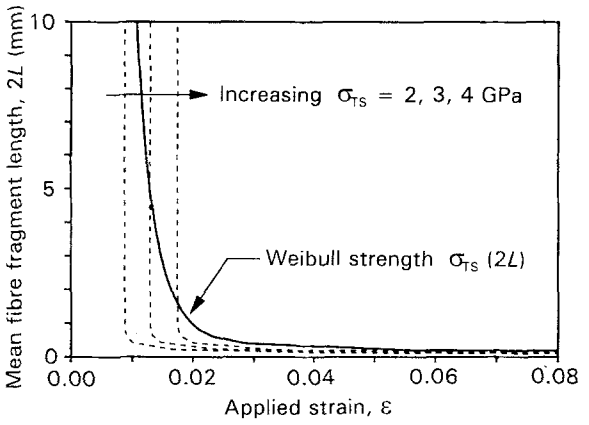

Figure 4 Variation of mean fibre fragment length, $2L$, versus applied strain, ε, in the full, bonded interface model, for (——) varying $\sigma_{TS}(2(L)$, and (– – –) constant fibre tensile strengths, σ_{TS}.

The mean fibre fragment length, $2L$, is plotted as a function of the applied strain, ε ($= \sigma/E_m$), in Fig. 4. Also superimposed are the results obtained when the fibre tensile strengths are assumed to be constant as given in Fig. 3b. The fully bonded model predicts that the mean fibre fragment length declines remarkably within a narrow range of applied strain, the decrease being instantaneous if a constant σ_{TS} is used, which is followed immediately by an almost constant value as the applied strain is further increased. The threshold value of the applied strain for the precipitous drop in

fibre fragment length increases with increasing constant, σ_{TS}. In contrast, there is no such threshold observed when σ_{TS} is given by the Weibull equation. It is also worth noting that the mean fibre fragment length becomes almost identical, regardless of whether the fibre tensile strength is Weibull-controlled or constant, when the applied strain is sufficiently large (Fig. 4).

However, it should be reiterated here that because Equation 34 is valid when the requirements of full bonding (given by Equation 33) are completely satisfied, only the initial declining part of the curves are effective at low applied strains in Fig. 4. The characteristic length, $(2L)_d$, which is maximum fibre length obtainable before debond initiation, is controlled strongly by the interface bond strength, τ_b, (Fig. 3a) as mentioned earlier. Therefore, unless τ_b is very large to prevent the interface from debonding (or, alternatively the matrix can withstand an extremely large strain), it is most unlikely that the fully bonded model can completely describe the relationship between mean fibre fragment length and applied strain during the whole fibre fragmentation process for practical fibre composites.

3.2. Partial debonding

In the fibre fragmentation test, the interfacial shear stress at the fibre ends quickly rises to a value corresponding to debonding as the applied stress increases. Plots of the fibre axial stress, $\sigma_f^z(z)/\sigma$, and the interfacial shear stress, $\tau_i^{rz}(z)/\sigma$, calculated based on Equations 1 and 2 for the bonded region and Equations 6 and 7 for the debonded region are shown in Fig. 5. Because a constant stress $\sigma = 117.4$ MPa (corresponding to initial debonding for $\tau_b = 72.7$ MPa) is applied to the composite of a given total fibre length $2L = 2$ mm, different debond lengths are shown for three different interface bond strengths, τ_b(= 50, 72.7 and 100 MPa). The fibre axial stresses are almost identical for these τ_b values, except near the boundary between the bonded and debonded regions where the stresses are high for a low τ_b. There is discontinuity of the interface shear stress at the boundary where the stress drop is large with a high τ_b (which is equivalent to the maximum stress just before the stress drop). In the debonded region, the interface shear stress increases non-linearly towards the fibre ends due to the small Poisson contraction of the fibre compared to the matrix under uniaxial tension.

The relationship between the applied stresses σ_{od} and σ_{of} is plotted as a function of normalized debond length, l/a, based on Equations 24 and 29 in Fig. 6 Only one curve is shown for σ_{od} in Fig. 6a, because it is almost independent of the mean fibre fragment length, $2L$. It is again demonstrated that when the fibre is sufficiently long it fractures without debonding (because $\sigma_{od} > \sigma_{of}$) until its length reaches a characteristic value $(2L)_d$. $(2L)_d = 2.71$ mm is obtained for $\tau_b = 72.7$ MPa by equating $\sigma_{od} = \sigma_{of}$ (i.e. $l = 0$, in Fig. 6a), which is exactly identical to the value determined in the previous section (Fig. 3a). Once debonding initiates it grows as fibre fragmentation

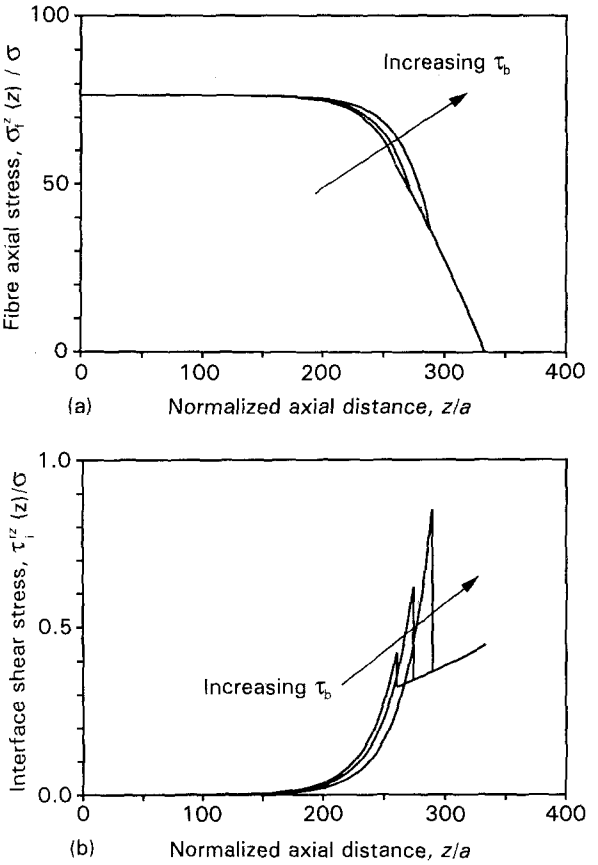

Figure 5 Distributions of (a) normalized fibre axial stress, σ_f^z/σ, and (b) normalized interface shear stress, τ_i^{rz}/σ, along the fibre axis, z/a, at a given applied stress $\sigma = 117.4$ MPa for $\tau_b = 50$, 72.7 and 100 MPa.

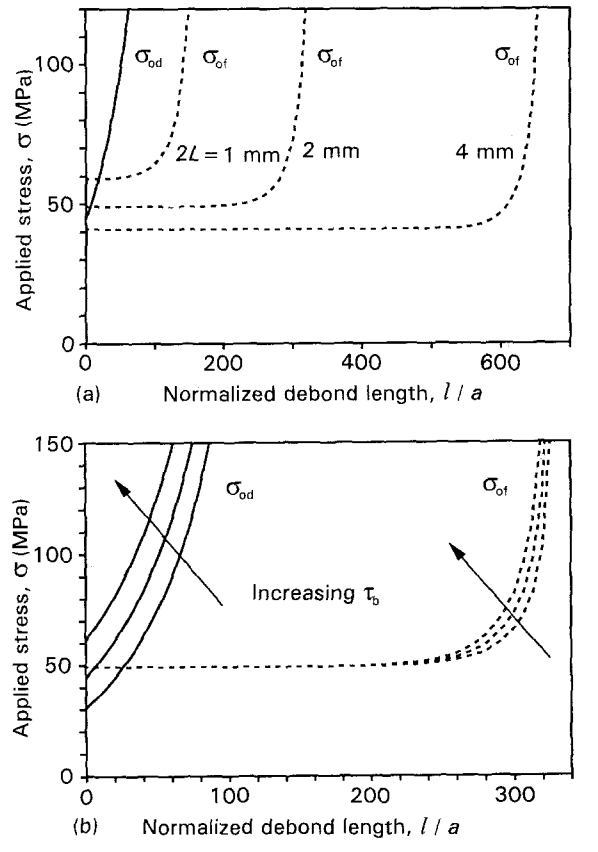

Figure 6 Plots of applied stresses required for (——) interfacial debonding, σ_{od}, and for (– – –) fibre fragmentation, σ_{of}, as a function of normalized debond length l/a: (a) for different fibre length $2L = 1$, 2 and 4 mm; (b) for different interface bond strength $\tau_b = 50$, 72.7 and 100 MPa.

continues. It is clear that both the fibre length corresponding to initial debonding, $(2L)_d$, and the debond length at a given applied stress are higher for the interface with a lower τ_b value (Fig. 6b). This is a direct result of the reduced stress required for debonding, σ_{od}, due to the low τ_b, whereas σ_{of} remains almost constant independent of τ_b.

The above accounts are correct when the interface conditions necessary for the partial debonding are completely satisfied, that is, the crack tip debond stress, σ_l, (and the debond length, l) must be greater than zero. From the debond criterion given by Equation 23

$$\sigma > \left(\frac{\alpha+\gamma}{1+\gamma}\right)\left(\frac{2}{a\beta_2}\right)\tau_b \coth[\beta_2(L-l)] \quad (35)$$

In the partially debonded model, whether debond continues or not depends strictly on the relative magnitude of the stresses required for debond propagation, σ_{od}, and for fibre fragmentation, σ_{of}, at a given debond length l. If σ_{od} given in Equation 24 is smaller than σ_{of} of Equation 29 interfacial debonding continues in preference to fibre fragmentation; and vice versa if σ_{od} is greater than σ_{of}. In conjunction with the general requirements of the partial debond model specified by Equation 35, the debond crack propagates when

$$\left(\frac{a\beta_2}{2}\right)\frac{[n_3+\nu_m n_1(\alpha+\gamma)]\,\sigma_{TS}(2L)+\alpha\nu_f(n_1+\lambda)\bar{\sigma}}{n_3\coth[\beta_2(L-l)]-[n_3+\nu_m n_1(\alpha+\gamma)]\,\mathrm{cosech}[\beta_2(L-l)]} > \tau_b > -\frac{\alpha\nu_f(n_1+\lambda)}{\nu_m n_1(\alpha+\gamma)}\left(\frac{a\beta_2}{2}\right)\sigma_{TS}(2L) \quad (36)$$

Similarly, the condition for fibre fragmentation is obtained from

$$\left(\frac{a\beta_2}{2}\right)\sigma_{TS}(2L)\frac{\sinh[\beta_2(L-l)]}{\cosh[\beta_2(L-l)]-1} > \tau_b > \left(\frac{a\beta_2}{2}\right)\frac{[n_3+\nu_m n_1(\alpha+\gamma)]\,\sigma_{TS}(2L)+\alpha\nu_f(n_1+\lambda)\,\bar{\sigma}}{n_3\coth[\beta_2(L-l)]-[n_3+\nu_m n_1(\alpha+\gamma)]\,\mathrm{cosech}[\beta_2(L-l)]} \quad (37)$$

Finally, the mean fibre fragmentation length $2L$, which is the sum of the debonded and bonded lengths in the partial debond model, can be determined from Equation 29

$$2L = 2l + (2/\beta_2)\sinh^{-1}\left\{\frac{2\tau_b/a\beta_2}{[(1+\gamma)/(\alpha+\gamma)]\,\sigma_{of}-\sigma_{TS}(2L)}\right\} \quad (38)$$

Therefore, a further study is made on the relationship between the applied stresses σ_{od} and σ_{of} with reference to Fig. 7 where τ_b is plotted versus the normalized debond length, l/a, for different fibre lengths using Equations 36 and 37. The solid lines represent the upper bounds for interface debond (which are also equivalent to the lower bounds for fibre fragmentation), and the dotted lines represent the upper bounds for fibre fragmentation. The lower bound curves for interface debonding are not shown here because the results are negative for the properties of the model composites being studied. There are three different regions identified: Region A for debonding only; Region B for fibre fragmentation without further debonding; Region C for neither debonding nor fibre fragmentation. It is found that if τ_b is greater than a certain value (i.e. $\tau_b = 94.7$ MPa for $2L = 1$ mm and $\tau_b = 78.8$ MPa for $2L = 2$ mm), further fibre fragmentation is not possible, although debonding can occur for a very short length. As the fibre length decreases, the upper bounds for both debond and fragmentation increase as a result of corresponding increase in the debond length for a given τ_b. There is a maximum debond length which is obtained before fibre fragmentation takes place for a given fibre length. This value can be determined systematically from the plot between the debond length, $2l$, versus the fibre length, $2L$, for a given τ_b shown in Fig. 8. This effectively means that there are alternating debond propagation and fibre fragmentation taking place during continuous loading in the fibre fragmentation test. In addition to the maximum fibre length corresponding to debond initiation, a minimum fibre length is also identified below which no further debond propagation occurs. The partial debond model is only effective for the range of fibre lengths between these limits where the debond length increases with decreasing fibre length (or increasing applied strain) for a given τ_b.

The above discussion for the partial debond model is summarized in Fig. 9 for two different τ_b values. The mean fibre fragment length, $2L$, consists of two components: namely the bond length $(2L - 2l)$, and the debond length $2l$. These two length components balance each other to determine the instantaneous mean fibre fragmentation length for a given applied strain. As the applied stress (or strain) increases, the debond length increases while the bond length decreases. Therefore, at low strains the bond length component dominates, but at high strains the debond length component becomes increasingly more important, eventually the latter outpacing the former (see Fig. 10). When the mean fibre fragment length is sufficiently short at a high applied strain, an infinitesimal increase in debond length or additionl fibre fragmentation requires the applied strain to suddenly increase toward an infinite value. This implies that a moderate (i.e. several-fold) increase in the applied strain at this stage would not cause any further fibre fragmentation. In practical fibre fragmentation tests, the mean fibre fragment length obtained after substantial increase in load application without further fibre fragmentation is called the critical transfer length. Therefore, the shortest mean fibre fragment length determined at the end of the curve shown in Fig. 9 can be regarded as the critical transfer length, $(2L)_c$, theoretically predicted

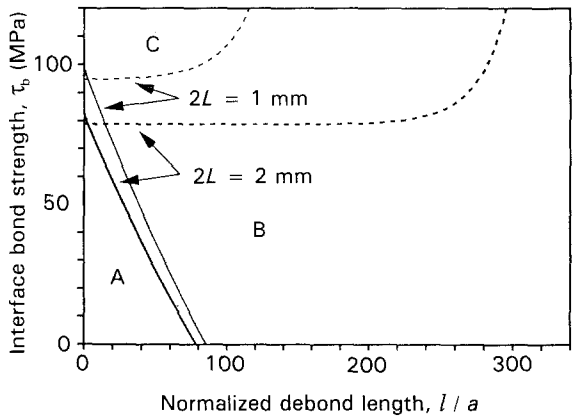

Figure 7 Plots of interface shear bond strengths, τ_b, as a function of normalized debond length, l/a, illustrating the areas corresponding to debonding only (Region A), fibre fragmentation without further debonding (Region B) and neither debonding nor fibre fragmentation (region C): (——) upper bound of Equation 36; (– – –) lower bound of Equation 37.

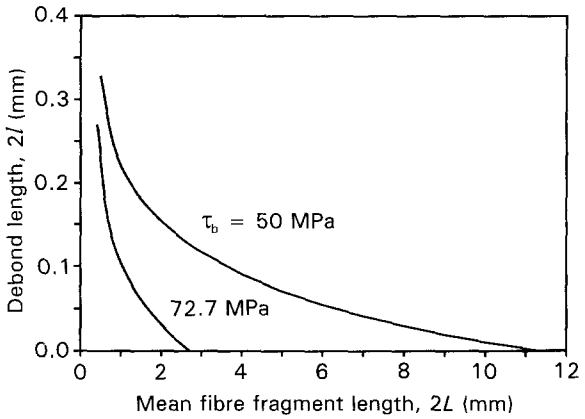

Figure 8 Variation of debond length, $2l$, plotted as a function of mean fibre fragment length, $2L$, predicted in the partially debonded interface model.

for the carbon fibre–epoxy matrix composite. It is also noted that the contribution of the debond length to the critical transfer length is slightly larger for the interface with a high bond strength (i.e. $l/L \approx 0.7$ and 0.67, respectively, for $\tau_b = 50$ and 72.7 MPa), while the converse is true for the critical transfer length, $(2L)_c$ (i.e. $(2L)_c \approx 0.47$ and 0.4 mm, respectively), if other parameters are kept the same.

3.3. Complete debonding (or full frictional bonding)

The condition for complete debonding at the interface requires that the fibre length and the debond length be identical, and the interfacial shear stress is maximum at the debond crack tip which now coincides with the fibre centre ($z = 0$). These requirements cannot be achieved in practice because the fibre axial stress has to be a maximum in the fibre centre whether the fibre is completely debonded or not. This means that the interfacial bond strength has to be zero ($\tau_b = 0$) which is rather impractical for most fibre composites. Alternatively, the fibre can be inherently mechanically bonded to the matrix, which is more likely to occur in some ceramic matrix composites [20]. In the latter

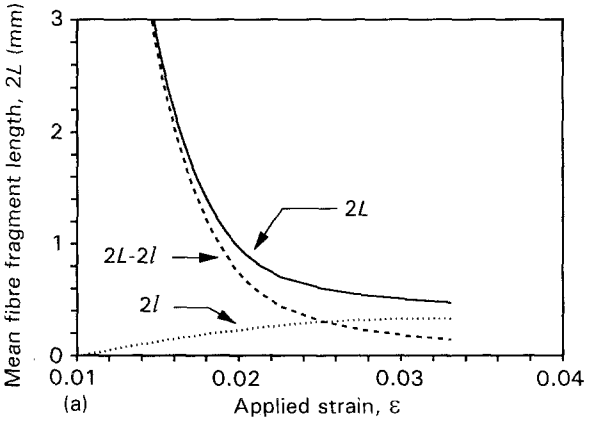

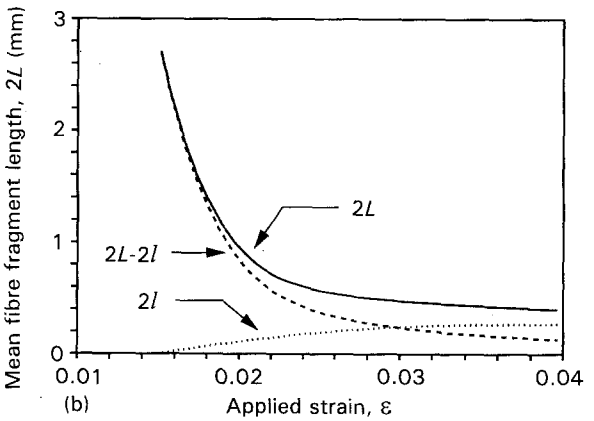

Figure 9 Variation of mean fibre fragmentation length, $2L$, versus applied strain, ε, in the partially debonded interface model for (a) $\tau_b = 50$ MPa, and (b) $\tau_b = 72.7$ MPa.

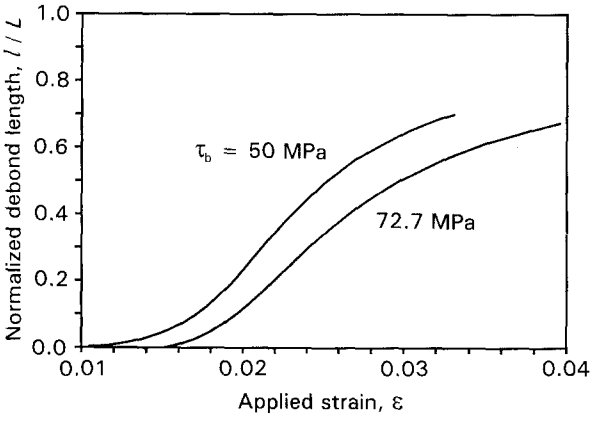

Figure 10 Plots of normalized debond length, l/L, as a function of applied strain, ε.

case, the interface shear stress is governed wholly by the Coulomb friction law, which is minimum in the centre where there is no Poisson contraction taking place and increases towards the fibre ends. Assuming the interface is fully frictionally bonded, the solutions for the fibre axial stress and the interfacial shear stress given by Equations 6 and 7 are still valid if the crack tip debond stress, σ_l, is substituted by the fibre axial stress at the centre, $\sigma_f^z(0)$, and $l = L$ for the non-dimensional coefficients D_i (where $i = 1, 2, 3, 4$) given in Equations 8–11.

$$\sigma_f^z(z) = \frac{B_3}{B_2}[D'_1 \exp(m_2 z) + D'_2 \exp(m_1 z)] + \sigma_f^z(0)\,[D'_3 \exp(m_2 z) + D'_4 \exp(m_1 z)] \quad (39)$$

$$\tau_i^{rz}(z) = -\frac{a}{2}\left\{\frac{B_3}{B_2}[m_2 D_1' \exp(m_2 z) + m_1 D_2' \exp(m_1 z)] + \sigma_f^z(0)\,[m_2 D_3' \exp(m_2 z) + m_1 D_4' \exp(m_1 z)]\right\} \tag{40}$$

where

$$D_i' = D_i]_{l=L} \tag{41}$$

$\sigma_f^z(0)$ can be determined for the boundary condition that the interfacial shear stress is minimum in the centre, i.e. $\tau_i^{rz}(0) = -\mu q_0$ and

$$\sigma_f^z(0) = \frac{\sigma[(1+\gamma)\nu_m/(\alpha\nu_f + \gamma\nu_m)](m_2 D_1' + m_1 D_2') + \omega\bar{\sigma}(\lambda + m_2 D_1' + m_1 D_2')}{m_2 D_3' + m_1 D_4'} \tag{42}$$

The fibre axial stress and the interface shear stress (normalized with the applied stress) are plotted along the axial direction, z/a, for varying residual clamping stress, q_0, as shown in Fig. 11. As expected, both the fibre axial stress and the interfacial shear stress distributions are higher for a larger q_0 value (in absolute terms) for a given fibre length. Varying the coefficient of friction, μ, would have similar effects on the stress distributions. The prevailing influence of differential Poisson contraction between the fibre and matrix is clearly seen in Fig. 11b where the interfacial shear stress increases, with the stress gradient becoming steeper, toward the fibre end. For the fully frictional model, the external stress corresponding to fibre fragmentation is then determined by equating Equation 42 directly to the fibre tensile strength, $\sigma_{TS}(2L)$.

$$\sigma_{of} = -\frac{\alpha\nu_f + \gamma\nu_m}{(1+\gamma)\nu_m}\,\frac{\sigma_{TS}(2L)\,(m_2 D_3' + m_1 D_4') + \omega\bar{\sigma}(\lambda + m_2 D_1' + m_1 D_2')}{m_2 D_1' + m_1 D_2'} \tag{43}$$

To satisfy the full frictional bonding condition at the interface, the applied stress σ_{of} given in Equation 43 must be at least greater than zero, which results in the fibre strength greater than a certain value for a given mean fibre fragment length, i.e.

$$\sigma_{TS}(2L) > \omega\bar{\sigma}\,\frac{\lambda + m_2 D_1' + m_1 D_2'}{(m_2 D_3' + m_1 D_4')} \tag{44}$$

In Fig. 12 the area above the solid line represents the combination of mean fibre fragment length and fibre tensile strength which satisfies the full frictional bonding at the interface during fibre fragmentation. It is seen that the full frictional interface model is valid for a small range of short fibre length if the average tensile strength model described by the Weibull statistics of Table I is used. The effective fibre tensile strength has to be greater than approximately 5.5 GPa for the properties of the composite being studied. Taking the aproximate values for the non-dimensional coefficients given in Equation 40, the solution for the mean fibre fragment length, $2L$, is given in a closed form equation

$$2L = -\frac{2}{m_2}\ln\left\{\frac{m_1(\alpha\nu_f + \gamma\nu_m)\sigma_{TS}(2L) + (\lambda - m_1)(\alpha\nu_f + \gamma\nu_m)\omega\bar{\sigma} - m_1\nu_m(1+\gamma)\,\sigma_{of}}{-(m_1 - m_2)\,[(\alpha\nu_f + \gamma\nu_m)\omega\bar{\sigma} - \nu_m(1+\gamma)\,\sigma_{of}]}\right\} \tag{45}$$

In Fig. 13 the mean fibre fragment length, $2L$, is plotted as a function of the applied strain, ε, based on Equation 45. To show clearly the general trend in a wide range of applied strain, several constant fibre tensile strengths are chosen for calculation. Analogous to the fully bonded model, the full frictional model predicts a continuous decrease (toward zero) of the mean fibre fragment length with increasing applied strain. A high fibre tensile strength results in a high applied strain required to initiate the fibre fragmentation. However, varying the constant fibre tensile strength does not much affect the mean fibre fragmentation length at a high applied strain.

4. Discussion

A major improvement of the present model relative to the earlier models [2, 12, 18] which are also based on a shear strength criterion for interfacial debonding is that the conditions required to satisfy the three different interfaces (i.e. full bonding, partial debonding and full frictional bonding [18]) are systematically identified. This allows the construction of a complete picture for the relationship between the mean fibre fragment length and the applied strain which is experimentally determined from the continuously monitored fibre fragmentation test. Moreover, by properly taking into account the differential Poisson contraction between the fibre and matrix which varies with both the axial position and the applied strain, it is shown that depending on the relative properties at the bonded and debonded interfaces the frictional shear stress increases from the boundary of the two regions toward the fibre ends. This effectively discourages debond propagation during the fibre fragmentation process, as opposed to the easy debond propagation due to the Poisson contraction of the fibre in the fibre pull-out test [20, 21]. Consequently, it is most unlikely to induce complete debonding along the whole fibre length even at very high applied strain in most practical polymer matrix composites.

Apart from the three different interface states discussed above, there is another state of "interphase" (as opposed to the "interface" which is conveniently assumed to have zero thickness), namely the yielding of matrix material immediately surrounding the cylindrical fibre. Plastic yielding occurs in the matrix instead of debonding at the fibre–matrix interface if the interface shear bond strength, τ_b, is sufficiently higher

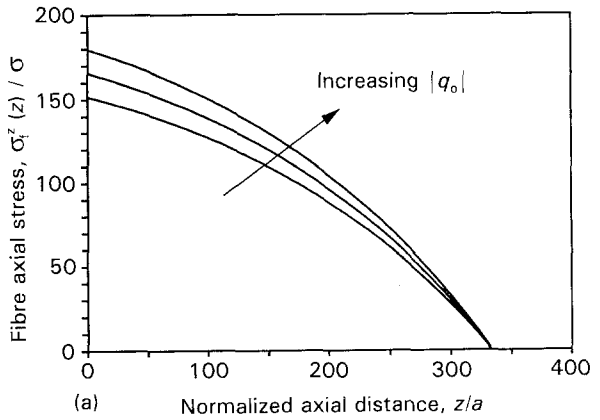

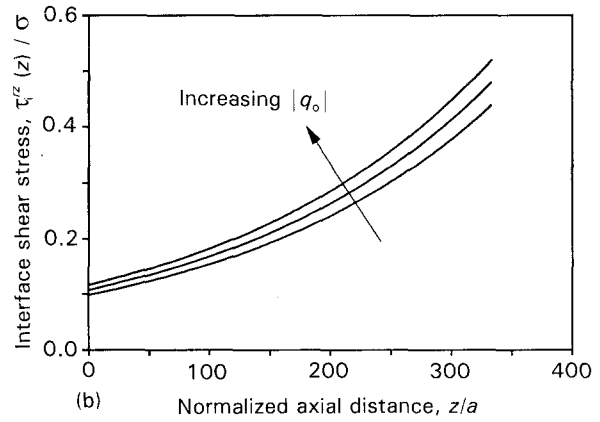

Figure 11 Distribution of (a) normalized fibre axial stress, σ_f^z/σ, and (b) normalized interface shear stress, τ_i^{rz}/σ, along the fibre axis, z/a, at a given applied stress for different residual clamping stresses $q_o = -7$, -10 and -13 MPa.

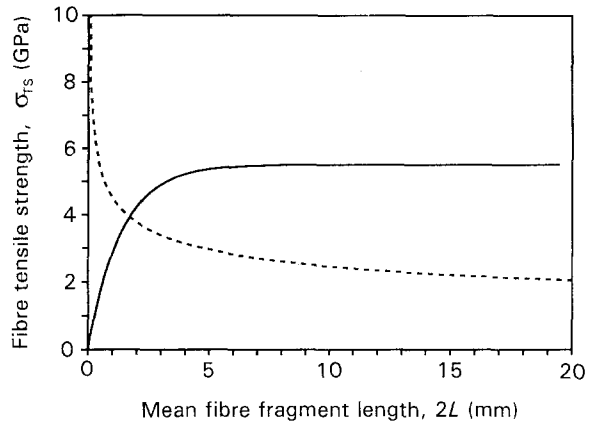

Figure 12 Plots of fibre tensile strength versus fibre length, $2L$: (——) calculated based on Equation 44; and (– – –) varying $\sigma_{TS}(2L)$ according to the Weibull parameters in Table I.

than the matrix yield strength in shear, τ_{my}, as in some composites containing ductile thermosets/thermoplastics and metal matrices. In the absence of the exact knowledge concerning the effective thickness of the interphase region being involved in plastic yielding and the elasto-plastic stress–strain behaviour of the matrix material, a detailed analysis is excluded in the present study. This would be one of the research areas which need further investigation to enhance understanding of the stress transfer in the fibre fragmentation test. It is noted that a constant matrix shear strength, τ_{my}, is assumed in a previous study [12].

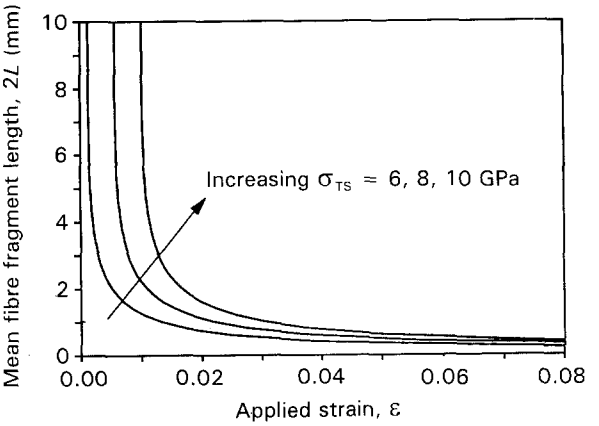

Figure 13 Variation of mean fibre fragment length, $2L$, as a function of applied strain, ε, predicted in the fully debonded interface model for constant fibre tensile strengths σ_{TS} = 6, 8 and 10 GPa.

There are other limitations of the present model, besides the assumption of perfectly elastic stress–strain behaviour for both the fibre and matrix: neglect of the anisotropy of fibre elastic properties and residual stresses in the axial direction (in addition to those in the radial direction) generated from the differential thermal contraction between fibre and matrix and a simplified fibre fracture criterion. In particular, with regard to the fibre strength model, it was assumed here that the fibre has uniform tensile strength along the fibre varying only with its length, and thus it fractures always in the centre due to the axisymmetric stress field. In practice, however, the fibre can break at any weak spots when the local stress exceeds the load-bearing capacity. The local stress is strongly influenced by the spatial distribution of the flaws of random sizes inherent on the brittle fibre surface which cannot be adequately accounted for in the average tensile strength model.

Within the limitations of the present micromechanics analysis, it is clearly demonstrated for a carbon fibre–epoxy matrix composite that one model cannot represent the interface state during the whole fibre fragmentation process. While the fully bonded interface model can describe the early stage of fibre fragmentation process (until the fibre length reaches a characteristic value $(2L)_d$ corresponding to initial debonding) for low applied strains, the interface soon becomes partially debonded as the applied strain increases, depending on the interface shear bond strength and the fibre tensile strength. Therefore, the mean fibre fragment length predicted for a given strain is the sum of the bonded and debonded lengths, the former diminishes while the latter grows with the applied strain, in the context of the partially debonded interface model. A non-zero critical value is always reached for the mean fibre fragment length when the applied strain required for further fibre fragmentation or interfacial debonding approaches infinity. Therefore, it is obvious that the critical transfer length, $(2L)_c$, can be considered as a material constant for given properties of the composite constituents and the interface. In reality, the critical transfer length, $(2L)_c$, is defined as the mean fibre fragment length determined after further substantial increment in the applied

strain leads to no additional fibre fragmentation, which is exactly the same as what is predicted by the present analysis. In view of the co-existence of bonded and debonded regions in the critical transfer length, $(2L)_c$, of vital importance in the fibre fragmentation experiment is the accurate measurements of their lengths which are absolutely necessary to characterize properly the relevant interfacial properties.

5. Conclusions

A micromechanics model is presented for the stress transfer in the single-fibre fragmentation test. Depending on the relative magnitude between the interface shear bond strength and the fibre tensile strength, three distinct interfaces are identified inclusive of full bonding, partial debonding and full frictional bonding. The conditions necessary to satisfy these interface conditions are also quantitatively evaluated as a function of the above two important parameters, which allow the relationship between the mean fibre fragment length and the applied strain to be established during the whole fibre fragmentation process.

The theoretical study for a model composite of carbon fibre–epoxy matrix shows that while the fully bonded interface model can describe the fibre fragmentation process for low applied strains, the partially debonded interface model is most suitable for the later stage for high applied strains. However, complete debonding is effectively discouraged due to the differential Poisson contraction between the fibre and matrix at the debonded interface. The mean fibre fragment length decreases with applied strain, reaching a critical value, $(2L)_c$, when the applied strain required for further fibre fragmentation approaches infinity. The critical transfer length can be regarded as a material constant which is totally consistent with the definition of a mean fibre fragment length in practice. In a broadly-based study, the present micromechanics model is extended to interpret adequately the fibre fragmentation test data, to be reported in Part II [22] of this paper. This allows the generation of useful interface properties for the carbon fibre–epoxy matrix composite with several different fibre surface treatments and matrix materials.

Acknowledgements

The authors thank the Australian Research Council (ARC) for continuing support of this work. J.K.K. is grateful for the Australian Postdoctoral Research Fellowship awarded by the ARC when this work was done and L.M.Z. is supported by a Sydney University Postgraduate Research Award.

Appendix 1. Stress transfer in the bonded region: $-(L-l) \leqslant z \leqslant (L-l)$

For perfectly elastic and isotropic fibre and matrix, the axial stresses, $\sigma_f^z(z)$ and $\sigma_m^z(r, z)$, and the matrix shear stress, $\tau_m^{rz}(r, z)$, can be related to the displacements by

$$\frac{\partial u_f^z(z)}{\partial z} = \frac{1}{E_f}\left\{\sigma_f^z(z) - \nu_f[\sigma_f^r(r, z) + \sigma_f^\theta(r, z)]\right\} \quad \text{(A1)}$$

$$\frac{\partial u_m^z(z)}{\partial z} = \frac{1}{E_m}\left\{\sigma_m^z(z) - \nu_m[\sigma_m^r(r, z) + \sigma_m^\theta(r, z)]\right\} \quad \text{(A2)}$$

$$\frac{\partial u_m^z(r, z)}{\partial r} = \frac{2(1+\nu_m)}{E_m}\tau_m^{rz}(r, z) \quad \text{(A3)}$$

where E and ν are Young's modulus and Poisson's ratio, respectively. The subscripts f and m refer to fibre and matrix and the superscripts are coordinate directions. It is assumed here that for a thin fibre the axial displacement is independent of the radial position, and the stress components in the radial and circumferential directions are neglected for Equations A1 and A2. Further, in Equation A3 for the matrix shear strain, the radial displacement gradient with respect to the axial direction is neglected as compared to the axial displacement gradient with respect to the radial direction. Also, the mechanical equilibrium condition between the external stress, σ, and the internal stress distribution requires that

$$b^2\sigma = a^2\sigma_f^z(z) + 2\int_a^b r\,\sigma_m^z(r, z)\,dr \quad \text{(A4)}$$

The external stress is transferred to the fibre through the interfacial shear stress $\tau_i^{rz}(z)$, and the equilibrium between these stresses is described by

$$\frac{d\sigma_f^z(z)}{dz} = -\frac{2}{a}\tau_i^{rz}(z) \quad \text{(A5)}$$

Therefore, the shear stress in the matrix, $\tau_m^{rz}(r, z)$, can be expressed as a function of the interfacial shear stress, $\tau_i^{rz}(z)$, analogous to the fibre pull-out problem [8]

$$\tau_m^{rz}(r, z) = \frac{\gamma(b^2 - r^2)}{ar}\tau_i^{rz}(z) \quad \text{(A6)}$$

Combination of Equations A3 and A6 for the boundary condition of axial displacement continuity at the bonded interface (i.e. $u_m^z(a, z) = u_f^z(z)$) and integration give

$$\tau_m^{rz}(r, z) = \frac{\gamma(b^2 - r^2)}{ar}\frac{E_m[u_m^z(b, z) - u_f^z(z)]}{2a(1+\nu_m)[(1+\gamma)\ln(b/a) - 1/2]} \quad \text{(A7)}$$

$$\tau_i^{rz}(z) = \frac{E_m[u_m^z(b, z) - u_f^z(a, z)]}{2a(1+\nu_m)[(1+\gamma)\ln(b/a) - 1/2]} \quad \text{(A8)}$$

Based on the relations between the stress components and the axial displacements given in Equations A1 and A2, the axial stress in the matrix can be derived from Equations A3 and A7

$$\sigma_m^z(r, z) = \sigma_m^z(a, z) + \frac{[b^2\ln(r/a) - (r^2 - a^2)/2]\,[\sigma_m^z(b, z) - \sigma_m^z(a, z)]}{(b^2 - a^2)[(1+\gamma)\ln(b/a) - 1/2]} \quad \text{(A9)}$$

where $\sigma_m^z(a, z)$ ($= \alpha\,\sigma_f^z(z)$) and $\sigma_m^z(b, z)$ are the matrix axial stresses at the inner ($r = a$) and outer ($r = b$) surfaces, respectively. Further, combination of Equation A8 with the mechanical equilibrium equa-

tion A4 yields

$$\sigma_m^z(b, z) = \sigma_f^z(z)\,[\alpha - 1/(\beta_1^2\gamma) - \alpha/(\beta_1^2\gamma^2)^2] + \sigma(1 + \gamma)/(\beta_1^2\gamma^2) \quad \text{(A10)}$$

where

$$\beta_1^2 = \frac{b^4 \ln(b/a) - (b^2 - a^2)^2/2 - (b^4 - a^4)/4}{a^4[(1 + \gamma)\ln(b/a) - 1/2]} \quad \text{(A11)}$$

Therefore, combining Equations A5 and A8–A10 yields a differential equation for the fibre axial stress $\sigma_f^z(z)$ as

$$\frac{d^2\sigma_f^z(z)}{dz^2} = \beta_2^2\left[\sigma_f^z(z) - \sigma\left(\frac{1 + \gamma}{\alpha + \gamma}\right)\right] \quad \text{(A12)}$$

where the coefficient β_2 is a function of the elastic properties and geometric factors of the constituents and is given in Equation 3. The solution of Equation A12 is subjected to the following boundary conditions for partially debonded fibre–matrix interface as a general case

$$\sigma_f^z(\pm(L - l)) = \sigma_l \quad \text{(A13)}$$

where σ_l is defined as the crack tip debond stress at the boundary between the bonded and debonded regions. From the solution of fibre axial stress $\sigma_f^z(z)$ as given in Equation 1, the corresponding interfacial shear stress $\tau_i^{rz}(z)$ is obtained in Equation 2.

Appendix 2. Stress transfer in the debonded region: $-L \leqslant z \leqslant -(L - l)$ and $(L - l) \leqslant z \leqslant L$

Because the interfacial shear stress, $\tau_f^{rz}(z)$, is the highest at the ends of the embedded fibre, debonding is expected to commence from the ends. In the debonded region frictional slip occurs at the interface where the stress transfer is governed by the Coulomb friction law. Assuming a constant coefficient of friction, μ, along the debonded interface it follows in the debonded region $(L - l \leqslant z \leqslant L)$ that

$$\tau_i^{rz}(z) = -\mu[q_0 + q^*(z)] \quad \text{(A13)}$$

where q_0 is the residual clamping stress (compressive) caused by the matrix shrinkage and differential thermal contraction (or expansion) of the constituents occurring during fabrication of the composite. $q^*(z)$ is the additional radial stress at the interface arising from the differential Poisson contraction between the fibre and matrix which is subjected to tension. According to Gao *et al.* [23] the solution for this additional stress is

$$q^*(z) = \frac{\alpha\nu_f\,\sigma_f^z(z) - \nu_m\,\sigma_m^z(a, z)}{\alpha(1 - \nu_f) + 1 + \nu_m + 2\gamma} \quad \text{(A14)}$$

Combining Equations A13 and A14 with the relationship between the fibre axial stress, $\sigma_f^z(z)$, and the interfacial shear stress, $\tau_i^{rz}(z)$, in Equation A5 gives the matrix axial stress at the interface, $\sigma_m^z(a, z)$

$$\sigma_m^z(a, z) = -\left(\frac{\alpha\nu_f + \gamma\nu_m}{\nu_m}\right)\left(\frac{d\sigma_f^z}{\lambda\,dz} + \omega\bar{\sigma}\right) + \frac{\alpha\nu_f}{\nu_m}\sigma_f^z \quad \text{(A15)}$$

Therefore, combination of Equations A4, A8, A9 and A15 yields a differential equation for the fibre axial stress

$$\frac{d^2\sigma_f^z}{dz^2} + B_1\frac{d\sigma_f^z}{dz} - B_2\,\sigma_f^z = B_3 \quad \text{(A16)}$$

where the coefficients B_1, B_2 and B_3 are given in Equations 4, 5 and 6. The general solution of Equations A16 for the partially debonded interface in the region $(L - l \leqslant z \leqslant L)$ is subjected to the boundary conditions

$$\sigma_f^z(L - l) = \sigma_l \quad \text{(A17)}$$

$$\sigma_f^z(L) = 0 \quad \text{(A18)}$$

Therefore, the fibre axial stress, $\sigma_f^z(z)$, and the interfacial shear stress, $\tau_i^{rz}(z)$, are given in Equations 6 and 7, which hold for the positive axial direction (i.e. the right-hand part of the fibre in Fig. 1). The corresponding solutions valid for the negative axial direction are obtained by symmetry of the axial stress and antisymmetry of the interfacial shear stress with respect to the fibre centre.

References

1. J. K. KIM and Y. W. MAI, in "Structure and Properties of Fibre Composites", *Materials Science and Technology Series*, Vol. 13, edited by T. W. Chou (VCH, Weinheim, Germany, 1993) Ch. 6.
2. H. L. COX, *Br. J. Appl. Phys.* **3** (1952) 72.
3. L. T. DRZAL, M. J. RICH, J. D. CAMPING and W. J. PARK, in "35th Annual Technical Conference on Reinforced Plastics (Composites Institute, SPI, 1980), Paper 20-C.
4. W. D. BASCOM and R. M. JENSEN, *J. Adhes.* **19** (1986) 219.
5. A. S.WIMOLKIATISAK and J. P. BELL, *Polym. Compos.* **10** (1989) 162.
6. A. N. NETRAVLI, R. B. HENSTENBURG, S. L. PHOENIX and P. SCHWARTZ, *ibid.* **10** (1989) 226.
7. R. B. HENSTENBURG and S. L. PHOENIX, *ibid.* **10** (1989) 389.
8. B. YAVIN, H. E. GALLIS, J. SCHERF, A. EITAN and H. D. WAGNER, *ibid.* **12** (1991) 329.
9. G. MERLE and M. XIE, *Compos. Sci. Technol.* **40** (1991) 19.
10. J. C. FIGUEROA, T. E. CARNEY, L. S. SCHADLER and C. LAIRD, *ibid.* **42** (1991) 77.
11. L. S. SCHADLER, C. LAIRD and J. C. FIGUEROA, *J. Mater. Sci.* **27** (1992) 4024–4034.
12. M. R. PIGGOTT, "Load Bearing Fibre Composites" (Oxford, Pergamon, 1980) Ch. 5.
13. A. KELLY and W. R. TYSON, *J. Mech. Phys. Solids* **13** (1965) 329.
14. I. VERPOEST, M. DESAEGER and R. KEUNINGS, in "Controlled Interphases in Composite Materials", (Proc. ICCI-III), edited by H. Ishida (Elsevier Science, Cleveland, OH (1990) pp. 653–66.
15. J. P. FAVRE, P. SIGETY and D. JACQUES, *J. Mater. Sci.* **26** (1991) 189.
16. R. GULINO, P. SCHWARTZ and S. L. PHOENIX, *ibid.* **26** (1991) 6655.
17. N. MELANITIS, C. GALIOTIS, P. L. TETLOW and C. K. L. DAVIES, *J. Compos Mater.* **26** (1992) 574–610.

18. Th. LACROIX, B. TILMANS, R. KEUNINGS, M. DESAEGER and I. VERPOEST, *Compos. Sci. Technol.* **43** (1992) 379–387.
19. L. M. ZHOU, J. K. KIM, C. BAILLIE and Y. W. MAI, *ibid.*
20. J. K. KIM, C. BAILLIE and Y. W. MAI, *J. Mater. Sci.* **27** (1992) 3143.
21. L. M. ZHOU, J. K. KIM and Y. W. MAI, *ibid.* **27** (1992) 3155.
22. J. K. KIM, L. M. ZHOU and Y. W. MAI, *J. Mater. Sci.*, to be published.
23. Y. C. GAO, Y. W. MAI and B. COTTERELL, *J. Appl. Math. Phys. (ZAMP)* **39** (1989) 550.
24. S. VAN DER ZWAAG, *J. Test. Eval. (JTEVA)* **17** (1989) 292.

Received 15 March
and accepted 7 May 1993